

PACS numbers: 42.30.Wb; 81.07.–b; 87.63.L–
DOI: 10.1070/QE2014v044n07ABEH015487

Nanosensitive optical coherence tomography for the study of changes in static and dynamic structures

S. Alexandrov, H. Subhash, M. Leahy

Abstract. **We briefly discuss the principle of image formation in Fourier domain optical coherence tomography (OCT). The theory of a new approach to improve dramatically the sensitivity of conventional OCT is described. The approach is based on spectral encoding of spatial frequency. Information about the spatial structure is directly translated from the Fourier domain to the image domain as different wavelengths, without compromising the accuracy. Axial spatial period profiles of the structure are reconstructed for any volume of interest within the 3D OCT image with nanoscale sensitivity. An example of application of the nanoscale OCT to probe the internal structure of medico-biological objects, the anterior chamber of an *ex vivo* rat eye, is demonstrated.**

Keywords: *biomedical optics, optical coherence tomography, optical coherence Fourier tomography, nanoscales.*

1. Introduction

Most fundamental biological processes in living tissues, including the development of cancer, take their start from the structural changes at the scales of a few nanometers (nanoscale). In this regard, much attention is paid to the development of methods aimed at improving the resolution and sensitivity of modern imaging instruments. Fundamental resolution limit has been recently overcome, with several methods for super resolution implemented in practice [1–6]. However, almost all these methods require the use of special markers, allow the formation of only two-dimensional images and are not suited for the study of living tissues *in vivo*. At the same time it is becoming more and more evident that two-dimensional studies of biological structures often do not reflect the real situation that occurs in three-dimensional objects. The optical coherence tomograph, an optical analogue of ultrasound equipment, enables the formation of a noncontact three-dimensional image of the internal structure of the object [7] and is increasingly often used for imaging of the biomedical objects and their diagnosis [8–10]; on the other hand, the resolution and sensitivity to the structural changes of most tomographs is less than 10 μm and only for some systems the resolution reaches 1 μm.

Different approaches have been used to increase the efficiency of optical imaging techniques, including optical tomography [11, 12], methods for studying the microstructures that are smaller than the diffraction limit of optical system resolution [13–16], and new methods of optical coherence tomography. Light scattering spectroscopy has been used in OCT to study the three-dimensional morphology of the cell nuclei [17, 18]. Spectral characteristics of the objects were derived from OCT [19], and the authors of [20] studied molecules. A correlation method for imaging the vascular system has been recently developed at our laboratory [21]. An interference microscope with a synthesised aperture has been proposed to improve the resolution of the image areas outside the focal plane [22, 23]. Application of the phase-sensitive OCT for measuring vibrations in the auditory organs [24, 25] and studying the cornea [26] with nanoscale sensitivity has been demonstrated. A possibility of using OCT to register the changes in the nanostructured, weakly scattering media was discussed as well [27].

A new approach for the study of the internal structure of objects, based on the spectral encoding of spatial frequency (SESF), has demonstrated the possibility of obtaining information about the internal structure of scattering objects for any region of interest within a two-dimensional image with a nanoscale sensitivity to structural changes [28–30]. A theoretical analysis of the possibility of applying this approach to three-dimensional images has been conducted [31]. However, despite significant progress in the development of methods for studying the structure of objects at micro- and nanoscales, the investigation of a three-dimensional structure of strongly scattering objects at the nanoscales still represents a serious problem.

Recently, we have demonstrated one of the possible solutions to the problem, i.e., the use of a variant of OCT, nanosensitive to the spatial and temporal structural changes within the three-dimensional scattering objects [32]. In this paper we represent the extension of the theory of the method, elucidate the results of the studies confirming the nanosensitivity and demonstrate the possibility of using OCT to study the structural changes in the anterior chamber of the rat eye, including the cornea and iris.

2. Image formation in OCT

As is known, the structure of the object can be described by a three-dimensional function (commonly called the scattering potential)

$$U(\boldsymbol{r}) = \frac{1}{4\pi} k_0^2 [n^2(\boldsymbol{r}) - 1] \tag{1}$$

or by the Fourier transform of the scattering potential

$$F(\boldsymbol{K}) = \int U(\boldsymbol{r}) \exp(-\mathrm{i}\boldsymbol{K}\boldsymbol{r})\, \mathrm{d}^3 r, \tag{2}$$

S. Alexandrov, H. Subhash, M. Leahy National University of Ireland, Galway, Ireland; e-mail: sergey.alexandrov@nuigalway.ie

Received 6 March 2014; revision received 7 May 2014
Kvantovaya Elektronika **44** (7) 657–663 (2014)
Translated by M.A. Monastyrskiy

where $k_0 = 2\pi/\lambda_0$; n is refractive index; and $\boldsymbol{K}$ is scattering vector [33]. In the far field, for large values of the vector $\boldsymbol{r}$, we have

$$\boldsymbol{K} = \frac{2\pi n}{\lambda_0}(\boldsymbol{s} - \boldsymbol{s}_0), \tag{3}$$

where $\boldsymbol{s}$ and $\boldsymbol{s}_0$ are the unit vectors of the illuminating and scattered waves (Fig. 1a). In Cartesian coordinates the vector $\boldsymbol{K}$ can be represented as

$$\boldsymbol{K} = 2\pi(v_x\boldsymbol{i} + v_y\boldsymbol{j} + v_z\boldsymbol{k}), \tag{4}$$

where v_x, v_y and v_z are the spatial frequencies along the respective Cartesian axes.

In accordance with the Born approximation of the scalar scattering theory, if the object is illuminated by a monochromatic plane wave, the complex amplitude of the scattered wave in a given direction in the far-field region and for a fixed wavelength contains information only about a single Fourier component of the scattering potential (one spatial frequency) corresponding to the vector $\boldsymbol{K}$. At a fixed illumination angle, the end of each vector corresponds to a point on a sphere having the radius $R = n/\lambda_0$, which is called the Ewald sphere. If broadband light is used for illumination, then, at a fixed angle of illumination (Fig. 1a), the distribution of spatial frequencies in the far-field region can be represented as a set of the Ewald spheres of different diameters. An example of such spheres, when the object is illuminated along the z axis for $n = 1$ at different wavelengths is shown in Fig. 1b. The relationship between the spatial frequencies and wavelengths can be given in the form

$$v_x = n(\sin\alpha - \sin\theta)\cos\varphi/\lambda, \quad v_y = n(\sin\alpha - \sin\theta)\sin\varphi/\lambda, \tag{5}$$

$$v_z = n(\cos\theta + \cos\alpha)/\lambda, \tag{6}$$

where θ is the incidence angle; α is the scattering angle; and φ is the azimuth angle (Fig. 1).

Having measured the complex amplitudes of the Fourier components for all possible wavelengths and different directions of illumination and scattering, it is possible to form a three-dimensional Fourier transform of the scattering potential. After that, the scattering potential can be reconstructed using a three-dimensional inverse Fourier transform:

$$U(\boldsymbol{r}) = \frac{1}{(2\pi)^3}\int F(\boldsymbol{K})\exp(-\mathrm{i}\boldsymbol{K}\boldsymbol{r})\,\mathrm{d}^3K. \tag{7}$$

However, even if the complex amplitudes of the spatial frequencies are measured for all possible directions of illumination and scattering, the range of spatial frequencies will be limited, the scattering potential will be reconstructed in the approximation of the low-frequency filtering, and the obtainable limiting resolution will amount approximately to a half the wavelength [33].

It is seen from Fig. 1 and formula (6) that a one-to-one correspondence within a small scattering angle α exists between the spatial frequency v_z and the wavelength. Within the SESF-approach this correspondence is used for spectral encoding of the frequencies v_z and transmitting them from the Fourier region into each pixel of the image plane without loss of information [28–31, 34].

A possible solution to the inverse scattering problem was examined by Wolf [33, 35, 36]. The OCT method proposes a one-dimensional solution to this problem, when the Fourier components are registered only along the z axis (vertical dashed line in Fig. 1b). The image formation process in the Fourier OCT is based on the adaptation of the original three-dimensional formalism to the one-dimensional case [37]. Each wavelength in the registered complex spectrum corresponds to one spatial frequency v_z. In other words, the wavelength in this case serves as a 'vehicle' for spatial transmission of information through an optical system. The registered OCT-signal represents a distribution of the complex amplitudes of the frequencies v_z, and therefore the corresponding z-profile of three-dimensional scattering potential (depth profile) can be reconstructed by means of one-dimensional inverse Fourier transform.

In the OCT frame, the range of recorded spatial frequencies can be calculated by the formula

$$\Delta v_z = \frac{2n\Delta\lambda}{\lambda_1\lambda_2}, \tag{8}$$

where $\Delta\lambda = \lambda_2 - \lambda_1$ is spectral range. In the process of performing an inverse Fourier transform to reconstruct the original object, spatial information is integrated, and, as a consequence, the resulting resolution of the method and its sensi-

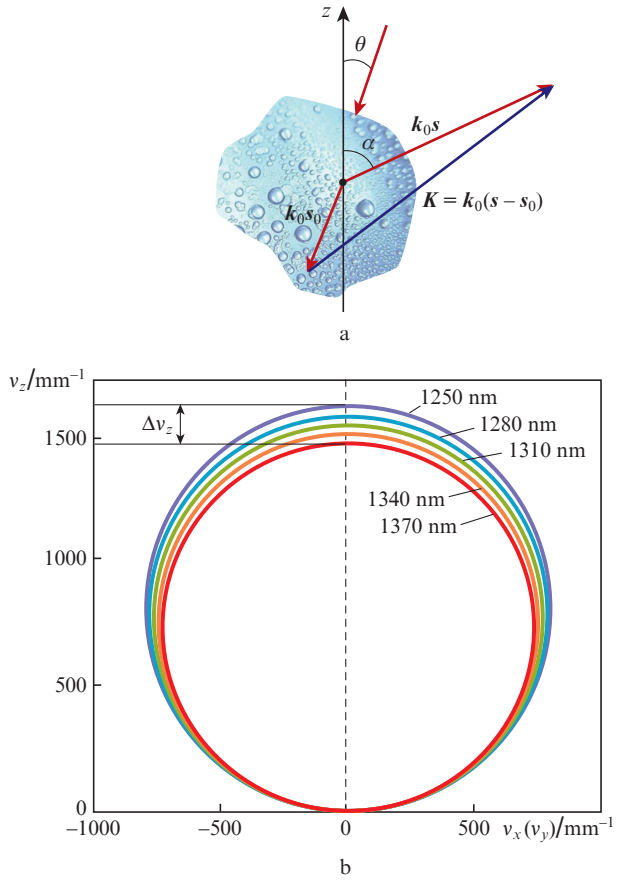

Figure 1. (a) Scheme of illumination of the object and scattering on it and (b) representation of spatial frequencies in the $\boldsymbol{K}$ space vs. the wavelength.

tivity to structural changes become significantly deteriorated. The depth resolution can be determined using the known formula [38]:

$$R_{z\mathrm{OCT}} = \frac{2\lambda_c^2 \ln 2}{n\pi\Delta\lambda}. \quad (9)$$

Thus, the resolution of the OCT and its sensitivity to structural changes within the object are limited by the scale of about a micrometer, and it is necessary to seek for new approaches to improve the sensitivity down to the nanoscales.

3. Nanosensitive OCT

The traditional way to increase the resolution and sensitivity consists, according to formula (9), in increasing the spectral range; however, it is impossible to attain the nanosensitivity in this case. Instead, we have proposed a completely new solution [32]. As is known, the Fourier spectrum of spatial frequencies is informative and sensitive to structural changes at the nanoscales [29, 30]. The SESF approach implies that the possession of information about the $\boldsymbol{K}$ space and image space allows exploration of small structural changes in the object by means of constructing a distribution of frequencies ν_z or spatial periods H_z for any region of two-dimensional image of interest. In the OCT frame, formula (6) can be rewritten as

$$\nu_z = \frac{2n}{\lambda}, \quad H_z = \frac{1}{\nu_z}. \quad (10)$$

Since the wavelength is spatially invariant, i.e., does not change in the course of the transformation from the $\boldsymbol{K}$ space into the image space, we can pass the spatial information into the image space lossless by means of encoding each spatial frequency (or period) in accordance with the appropriate wavelength (10), herewith maintaining the sensitivity to structural changes at the nanoscales.

For practical implementation of the method proposed, using formula (10), let us transform the complex recorded spectrum into the complex spectrum of spatial frequencies. After this, we divide the resulting complex spectrum of spatial frequencies into the sub-bands, while the image space – into the set of volumes, the internal structure of which we want to explore. Then we calculate the energy contribution I_m from the lth sub-band into the distribution of spatial periods H_{zl} for the mth volume:

$$I_m(H_{zl}) = \int_{V_m} |U_{ml}(\boldsymbol{r})|^2 \mathrm{d}\boldsymbol{r}, \quad (11)$$

where V_m is the volume of integration; $U_{ml}(\boldsymbol{r})$ is the inverse Fourier transform:

$$|U_{ml}(\boldsymbol{r})| = \frac{1}{(2\pi)^3} \int_{k_l} F(\boldsymbol{K}) \exp(\mathrm{i}2\pi \boldsymbol{K}\boldsymbol{r}_m)\, \mathrm{d}\boldsymbol{K}; \quad (12)$$

$\boldsymbol{r}_m$ indicates that the contribution of the lth sub-band of the spatial frequencies is considered only for the mth volume in the image space. By calculating the contribution $I_m(H_{zl})$ from all spatial periods H_{zl}, we reconstruct the z-profile of spatial periods for the mth volume inside the object. Thus, the information about the internal local structure can be visualised for every small volume within the three-dimensional image with a nanosensitivity to structural changes.

According to the relations that link the $\boldsymbol{K}$ space with image space, the sampling size in the $\boldsymbol{K}$ space determines the depth of the reconstructed image. Therefore the width of each sub-band of spatial frequencies determines the depth resolution, while the number of sub-bands – the number of points that are used to reconstruct the z-profiles of spatial periods. Consequently, we are facing here a compromise between the spatial resolution and the accuracy of reconstruction of structural information, wherein the best choice depends on the particular task. For a given range of spatial frequencies $\Delta\nu_{zl}$, the smallest size of the reconstructed volume in depth can be found by the formula

$$\Delta z = \frac{1}{2\Delta\nu_{zl}}. \quad (13)$$

The minimal longitudinal dimension of the object under consideration is determined by the lens resolution. We understand the sensitivity as the smallest changes in the z-profile of the spatial period, which still can be registered. The theoretical limit of the sensitivity to structural changes can be calculated by the formula

$$\delta H_z = \frac{\delta\lambda}{2n}, \quad (14)$$

where $\delta\lambda$ is the accuracy of the wavelength determination. Thus, if we know the wavelength with the accuracy of up to 1 nm, the sensitivity to the structural changes in the air amounts to about 0.5 nm.

Various parameters characterising the structure and dependent on the application can be calculated from the reconstructed z-profile of the spatial periods and represented as coloured images. For example, one such parameter may be the dominant spatial period that corresponds to the maximum signal value directly characterises the size of the dominant local structure.

4. Experiments and discussion of the results

In order to experimentally demonstrate the possibilities of our method, we used a conventional spectral OCT (Fig. 2). The light source was a broadband superluminescent diode with a centre wavelength of 1300 nm and a spectral range of 83 nm (DenseLight, Singapore). The spectrometer included a grating (1145 lines mm^{-1}) and a linearly scanning InGaAs camera (frequency of 91 kHz, 1024 pixels; S1024LDH2, Goodrich Ltd., USA). A helium–neon laser was used for the system adjustment. The frame rate was equal to 50 Hz when registering a two-dimensional OCT image (B-mode). The measured resolution along the depth in air was about 12 μm, while the transverse resolution – about 30 μm.

The images were formed as colour spatial distributions of dominant periods. In most experiments, the voxel size was 30×30×50 μm.

To experimentally test the sensitivity of the method to structural changes, we used a sample, which consisted of two layers of aggregated nanospheres made of polystyrene (Fig. 3). Each layer represented a strongly scattering multilayered three-dimensional structure, the spatial periods of which

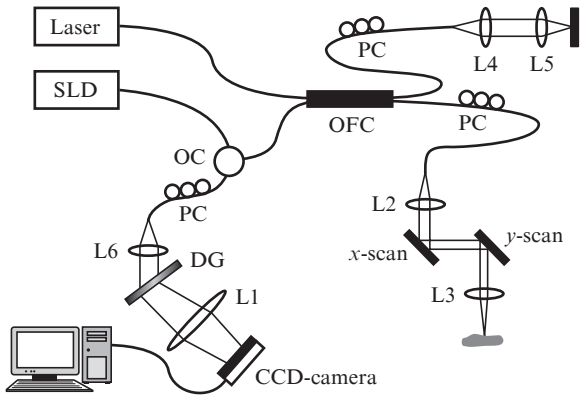

Figure 2. Scheme of the spectral optical coherence tomograph for the implementation of nanosensitive OCT:
(SLD) superluminescent diode; (DR) diffraction grating; (OC) optical circulator; (PC) polarisation controller; (OFC) optical fibre coupler; (L1 – L6) lenses.

depend on the size of the spheres, the refractive indices of the environment and the spheres, and their order. In other words, this sample represented a complex three-dimensional spatial structure and could serve as a model of biological tissue. The sample was examined using electron microscopy; the images of the spheres in the two layers are shown in Fig. 3. The measured diameters of the spheres constituted 614±18 nm and 644±20 nm, so that there was a probability that the spheres from different layers could have the same diameter.

In the OCT image (Fig. 4a) representing a cross section of the sample along the depth, the upper layer contains the spheres with an average size of 614 nm, while the lower layer – with an average size of 644 nm. The sizes of the spheres are much smaller than the resolution limit of the OCT we have used; therefore, it is impossible to see them, and all the more to register the difference in the structure of the layers. However, after reconstructing the z-profiles of the spatial periods of the structure for different areas within the sample by means of our method, we can see that the dominant spatial periods for the areas in the lower layer are greater than those for the areas inside the top layer [32]. The vertical dashed lines in Fig. 4a indicate the spatial periods at which the signal value attains its maximum (dominant periods). The increase in the dominant periods within the lower layer indicates that the size of the dominant structure in it is greater than in the upper layer, in accordance with the distribution of spheres in sizes in the layers, measured by electron microscopy. Figure 4b represents a colour distribution of the dominant spatial periods of the sample structure obtained. It can be seen that in most local areas at the bottom of the image (lower layer) the colours are shifted to red, which corresponds to a larger size of the dominant structure in these areas as compared to the upper part of the image (upper layer). Herewith, the difference in sizes of the dominant structures in layers is registered regardless of which layer is on the top [32]. This means that the approach developed by us is capable of registering the structural changes of 30 nm inside the sample by using only a single image (single scan).

This feature makes this approach very attractive in studies of the structural changes in time. We have shown that the structural changes in different areas of the object, having the size less than 30 nm, can be detected in time using this method [32]. In this paper, we investigate the possibility of its application to study the structural changes in the key areas of the anterior chamber of the rat eye, including the cornea and iris. Since the cornea is a weakly scattering object, the possibility of getting the image was not obvious. To demonstrate this possibility, we used eight-to-twelve week old Sprague-Dawley rats (CD, Harlan Laboratories, UK). All procedures performed on animals were approved by the Animal Ethics Committee of the National University of Ireland, Galway, and conducted in accordance with a license of the Department of Health in Ireland and the Standard Operating Procedures of the Animal Facility at the National Centre for Biomedical Engineering Science, Galway, Ireland. After euthanasia of the rat through the carbon dioxide inhalation, her eyes were removed and placed in a plastic container filled with a biological solution (PBS).

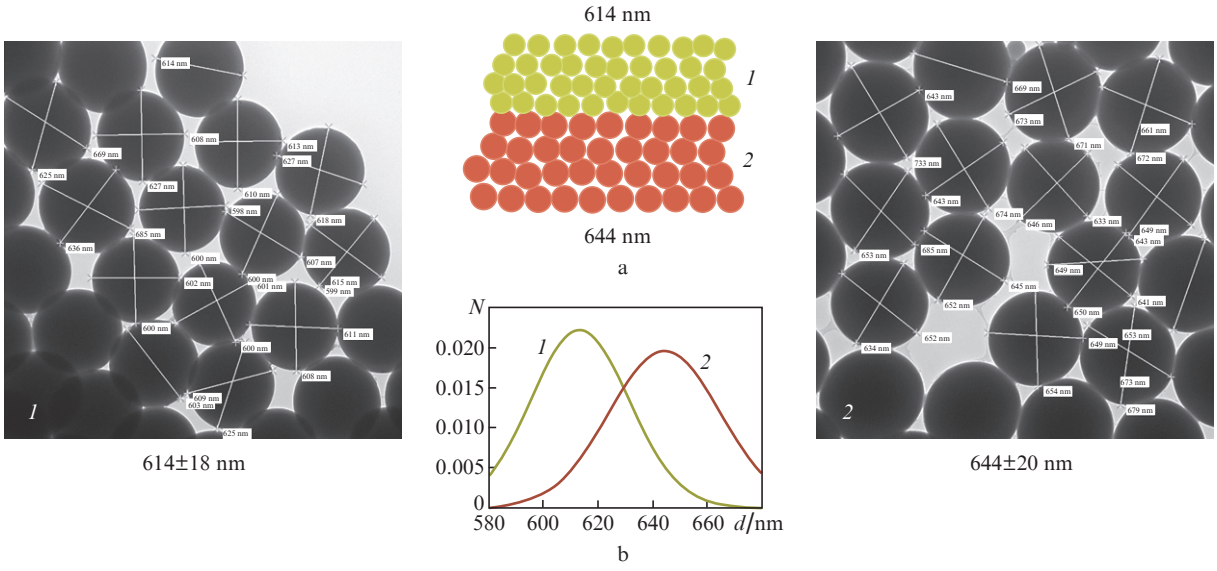

Figure 3. (a) Scheme of the sample with the corresponding photographs of the structure in two layers and (b) the distribution of spheres in the size d of these layers. The images and distributions are obtained using electron microscopy.

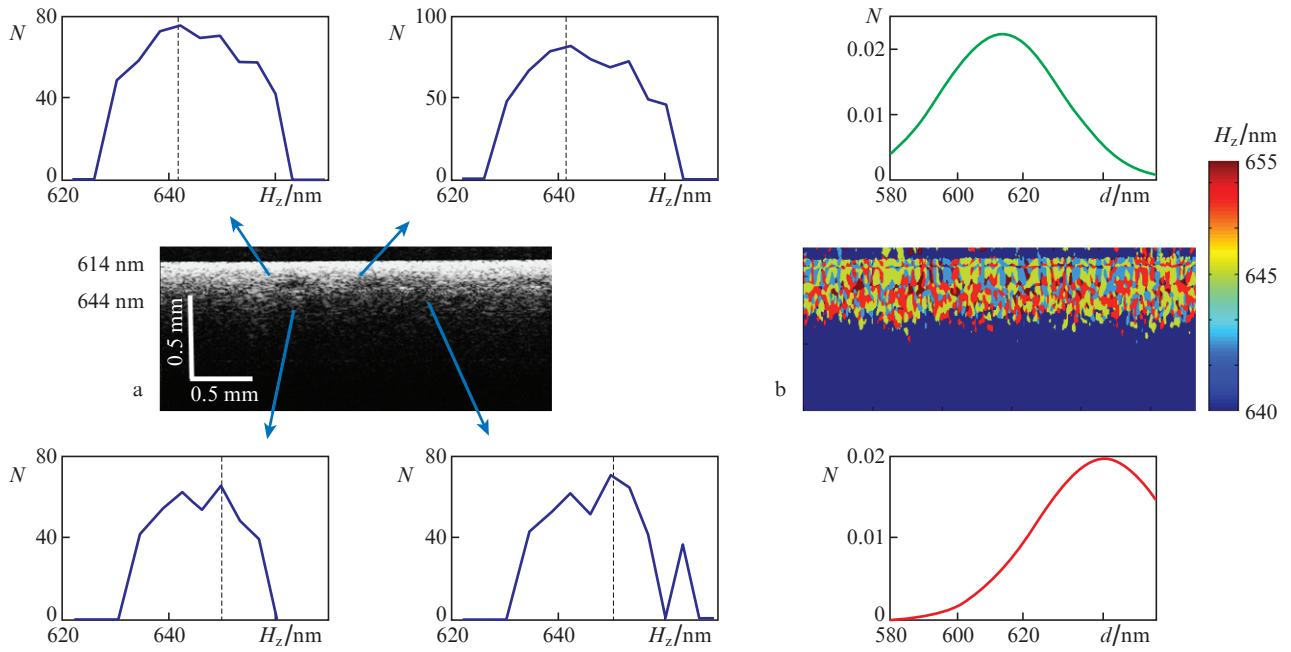

Figure 4. Images of a two-layer sample: (a) the conventional OCT image with the z-profiles of spatial periods for two local areas and (b) the image of the dominant structure with the distributions of spheres in layers relative to sizes, obtained with the nanosensitive OCT and measured by electron microscope. A colour version of Fig. 4 (as well as Figs 5 and 6) is available online at http://www.quantum-electron.ru.

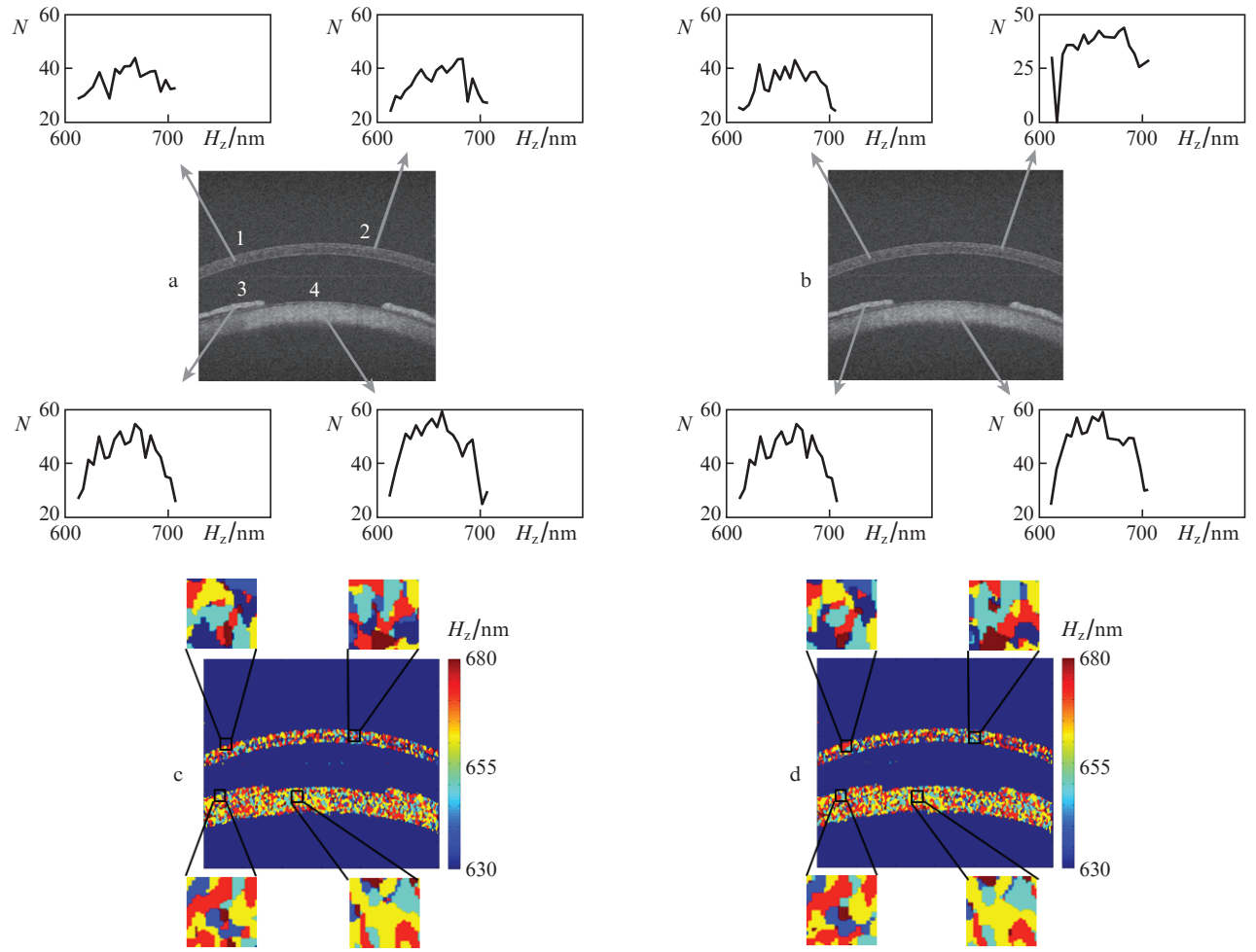

Figure 5. Images of the anterior chamber of the rat eyes: (a, b) the OCT images with z-profiles of spatial periods for two local areas and (c, d) the OCT images obtained with our method. The time interval between the registration of the images in Figs 5a, c and in Figs 5b, d constituted 20 ms.

Structural changes within the eye were taking place as a result of natural drying and dehydration. The time interval between the image registration in Figs 5a, c and Figs 5b, d is equal to 20 ms. Comparing the conventional OCT images (Figs 5a and 5b), it is impossible to see any change in the structure during this time interval. However, applying the approach we have developed and constructing the z-profiles of the internal structure of spatial periods for different local areas inside the cornea and iris, it is possible to visualise structural changes. Comparing the profiles of spatial periods, it can be concluded that the changes in structure inside the iris (area 3) are negligible, while the structure of the cornea (regions 1 and 2) experience significant changes. Such structural changes are clearly visible in Figs 5c, d and the enlarged image areas 2 and 3 in Fig. 6. All the colour area in Figs 6a and 6b have roughly the same dimensions and shape, while the coloured area in Figs 6c and 6d are significantly different in shape and size. For example, the dark red area in the image centre in Fig. 6a remains in Fig. 6b, only slightly increased in size. Herewith, the blue area in the centre of Fig. 6c substantially alters the size and shape in Fig. 6d. Even the correlation coefficients between the images in Figs 6a, b and Figs 6c, d, averaged over the three colour channels (R, G, B), are significantly different and amount, respectively, to 0.8 and 0.6. It follows from the data obtained that the process of dewatering primarily causes changes in the structure of the cornea.

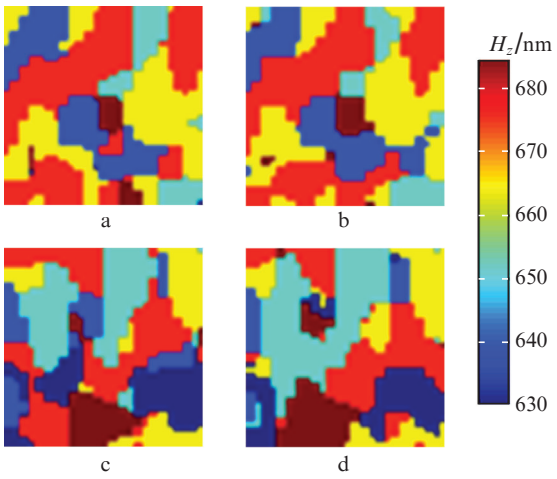

Figure 6. Enlarged images (see Figs 5c, d) of the anterior chamber of the rat eye for region 3 inside the iris (a, b) and region 2 inside the cornea (c, d). The time interval between the registration of the images in Figs 6a, c and Figs 6b, d is 20 ms.

The results of experiments have shown that our approach can be successfully applied for the study of small structural changes within the anterior chamber of the rat eye. This opens up good prospects of its application in the studies of the structural changes resulted from various influences, e.g. introduction of stem cells into the cornea.

5. Conclusions

We have developed a new approach that can significantly improve the sensitivity of OCT to structural changes within the highly scattering media. An advanced theory is represented, and it is shown that the application of the spectral encoding of spatial frequency along the object depth and transformation of spatial information directly from the Fourier region into the image space without loss of sensitivity allows registering the nanostructure changes. The possibility of applying this approach for studying the biomedical objects is demonstrated by means of investigating the structural changes in the anterior chamber of the rat eye in the process of its dewatering. The experiments have shown that this approach can be also used to study weakly scattering objects (cornea). This opens up good prospects for its further application in the studies of the processes associated with the structural changes in the eye, as example, the regeneration processes resulted from the introduction of the stem cells.

References

1. Cotte Y. et al. *Nat. Photonics*, **7**, 113 (2013).
2. Wang Z. et al. *Nat. Commun.*, **2**, 1 (2011); http://www.natur.com/ncomms/journal/v2/n3/full/ncomms1211.html.
3. Gustafsson M.G. *Proc. Nat. Acad. Sci. USA*, **102**, 13081 (2005).
4. Hell S.W. *Nat. Biotechnol.*, **21**, 1347 (2003).
5. Sheppard C. *Micron*, **38**, 165 (2007).
6. Sentenac A., Chaumet P.C., Belkebir K. *Phys. Rev. Lett.*, **97**, 243901 (2006).
7. Huang D. et al. *Science*, **254**, 1178 (1991).
8. Adler D.C. et al. *Nat. Photonics*, **1**, 709 (2007).
9. Liu L.B. et al. *Nat. Med.*, **17**, 1010 (2011).
10. Vakoc B.J. et al. *Nat. Med.*, **15**, 1219 (2009).
11. Sharpe J. et al. *Science*, **296**, 541 (2002).
12. Maire G. et al. *Phys. Rev. Lett.*, **102**, 213905 (2009).
13. Alexandrov S.A., Hillman T.R., Gutzler T., Sampson D.D. *Phys. Rev. Lett.*, **97**, 168102 (2006).
14. Alexandrov S.A., Hillman T.R., Sampson D.D. *Opt. Lett.*, **30**, 3305 (2005).
15. Hillman T.R., Gutzler T., Alexandrov S.A., Sampson D.D. *Opt. Express*, **17**, 7873 (2009).
16. Mico V., Zalevsky Z., Ferreira C., Garcia J. *Opt. Express*, **16**, 19260 (2008).
17. Graf R.N., Wax A. *Opt. Express*, **13**, 4693 (2005).
18. Pyhtila J.W., Wax A. *Opt. Express*, **12**, 6178 (2004).
19. Robles F., Graf R.N., Wax A. *Opt. Express*, **17**, 6799 (2009).
20. Robles F.E., Wilson C., Grant G., Wax A. *Nat. Photonics*, **5**, 744 (2011).
21. Enfield J., Jonathan E., Leahy M. *Biomed. Opt. Express*, **2**, 1184 (2011).
22. Ralston T.S., Marks D.L., Carney P.S., Boppart S.A. *Nat. Phys.*, **3**, 129 (2007).
23. Ralston T.S., Adie S.G., Marks D.L., Boppart S.A., Carney P.S. *Opt. Lett.*, **35**, 1683 (2010).
24. Chen F. et al. *Nat. Neurosci.*, **14**, 770 (2011).
25. Subhash H.M. et al. *J. Biomed. Opt.*, **17**, 060505 (2012).
26. Choi W. et al. *Opt. Lett.*, **38**, 338 (2013).
27. Yi J. et al. *Opt. Express*, **21**, 9043 (2013).
28. Alexandrov S.A., Sampson D.D. *J. Opt. A: Pure Appl. Opt.*, **10**, 025304 (2008).
29. Alexandrov S.A., Uttam S., Bista R.K., Zhao C.Q., Liu Y. *Opt. Express*, **20**, 9203 (2012).
30. Alexandrov S.A., Uttam S., Bista R.K., Staton K., Liu Y. *Appl. Phys. Lett.*, **101**, 033702 (2012).
31. Uttam S., Alexandrov S.A., Bista R.K., Liu Y. *Opt. Express*, **21**, 7488 (2013).
32. Alexandrov S., Subhash H.M., Zam A., Leahy M. *Nanoscale*, **6**, 3545 (2014).
33. Born M., Wolf E. *Principles of Optics: Electromagnetic Theory of Propagation, Interference and Diffraction of Light* (Cambridge: Cambridge University Press, 1999).
34. Alexandrov S.A., Uttam S., Bista R.K., Liu Y. *Opt. Lett.*, **36**, 3323 (2011).

35. Wolf E. *Opt. Commun.*, **1**, 153 (1969).
36. Wolf E. *J. Opt. Soc. Am.*, **59**, 482 (1969).
37. Fercher A.F., Hitzenberger C.K., Kamp G., Elzaiat S.Y. *Opt. Commun.*, **117**, 43 (1995).
38. Xi P., Mei K., Bräuler T., Zhou C., Ren Q. *Appl. Opt.*, **50**, 366 (2011).